Lithos 320–321 (2018) 403–415

Contents lists available at ScienceDirect

Lithos

journal homepage: www.elsevier.com/locate/lithos

Early Neoproterozoic (ca. 900 Ma) rift sedimentation and mafic magmatism in the North Lhasa Terrane, Tibet: Paleogeographic and tectonic implications

Pei-yuan Hu [a,b,*], Qing-guo Zhai [a], Guo-chun Zhao [c,b], Jun Wang [a], Yue Tang [a], Hai-tao Wang [a], Zhi-cai Zhu [a], Wei Wang [a], Hao Wu [a]

[a] Key Laboratory of Deep-Earth Dynamics of Ministry of Natural Resources, Institute of Geology, Chinese Academy of Geological Sciences, Beijing 100037, China
[b] State Key Laboratory of Continental Dynamics, Department of Geology, Northwest University, Xi'an 710069, China
[c] Department of Earth Sciences, University of HongKong, Pokfulam Road, Hong Kong, China

ARTICLE INFO

Article history:
Received 27 June 2018
Accepted 30 September 2018
Available online 3 October 2018

Keywords:
Tibet
North Lhasa terrane
Detrital zircon dating
Petrogenesis
Rift
Early Neoproterozoic

ABSTRACT

The origin and evolution of the Precambrian North Lhasa Terrane in the central Tibetan Plateau remain enigmatic. Here we present U—Pb age and Hf isotopic data for detrital zircons from early Neoproterozoic quartzites in the North Lhasa Terrane, Tibet. An integrated petrological, geochronological, geochemical, and Sr–Nd–Hf isotopic study was also undertaken on amphibolites associated with the quartzites. The depositional age of the quartzites is constrained to be between ca. 931 Ma (youngest detrital igneous zircon core) and 869 Ma (oldest metamorphic zircon rim). The detrital zircons have a main age population from 1200 to 1000 Ma, and lack zircons with ages of 1000–900 Ma. Zircons from the amphibolites yield concordant ages of ca. 913–902 Ma, which are comparable to the depositional age of the quartzites. The amphibolites have N-MORB-like compositions and are characterized by high positive zircon $\varepsilon_{Hf}(t)$ (+7.2 to +14.0) and whole-rock $\varepsilon_{Nd}(t)$ (+5.5 to +6.0) values. Their compositions have been modified by crustal contamination. The formation of these quartzites and amphibolites was related to an early Neoproterozoic rift adjacent to the African side of the northern East African Orogen, followed by opening of part of the Mozambique Ocean.

1. Introduction

The Tibetan Plateau marks the eastern end of the Himalayan–Alpine orogenic belt and records the tectonic processes of continental rifting, drifting, subduction, and collision (e.g., Allègre et al., 1984; Yin and Harrison, 2000). It is widely accepted that the Tibetan Plateau is a complex tectonic collage resulting from a number of continental collisional events between Gondwana-derived terranes (e.g., the South Qiangtang, North Lhasa, and South Lhasa terranes; Fig. 1a) and/or continents (e.g., India) since the early Paleozoic (Yin and Harrison, 2000). Previous studies have focused on the Phanerozoic tectonic evolution of the Tibetan terranes (e.g., Wang et al., 2008), with only limited research on their Precambrian origin and evolution.

The North Lhasa Terrane is one of the main components of the Tibetan Plateau (Yang et al., 2009; Zhang et al., 2012) and its origin is poorly understood (e.g., Allègre et al., 1984; Audley-Charles, 1984). The conventional view was that the North Lhasa Terrane originated from northeastern India and shares a similar origin to the South Lhasa and South Qiangtang terranes (e.g., Allègre et al., 1984; Gehrels et al., 2011; Yin and Harrison, 2000). Subsequently, detrital zircon data of Paleozoic metasedimentary rocks indicate that the North Lhasa Terrane originated from northern Australia and experienced a different Precambrian–early Paleozoic evolution to that of the South Qiangtang–South Lhasa–India system (Zhu et al., 2011a). Furthermore, new zircon U—Pb ages and whole-rock geochemical data of middle–late Neoproterozoic metamorphic (Dong et al., 2011; Zhang et al., 2012, 2013) and arc-related igneous (Hu et al., 2018a, 2018b, 2018c; Zhang et al., 2013) rocks indicate that the North Lhasa Terrane was part of the northern East African Orogen (EAO).

The Nyainqentanglha Group is widespread throughout the North Lhasa Terrane and is generally considered to be its Precambrian basement (Dong et al., 2011; Hu et al., 2016; Zhang et al., 2012). Early Neoproterozoic mafic meta-igneous rocks (ca. 925–886 Ma; Zhang et al., 2012; Hu et al., 2016) have been documented in the Nyainqentanglha Group, but their petrogenesis remains poorly understood. These mafic rocks represent the oldest magmatism in the North Lhasa Terrane and are therefore essential in constraining the

* Corresponding author at: Key Laboratory of Deep-Earth Dynamics of Ministry of Natural Resources, Institute of Geology, Chinese Academy of Geological Sciences, 26 Baiwanzhuang Road, Beijing 100037, China.
E-mail address: azure_jlu@126.com (P. Hu).

https://doi.org/10.1016/j.lithos.2018.09.036
0024-4937/

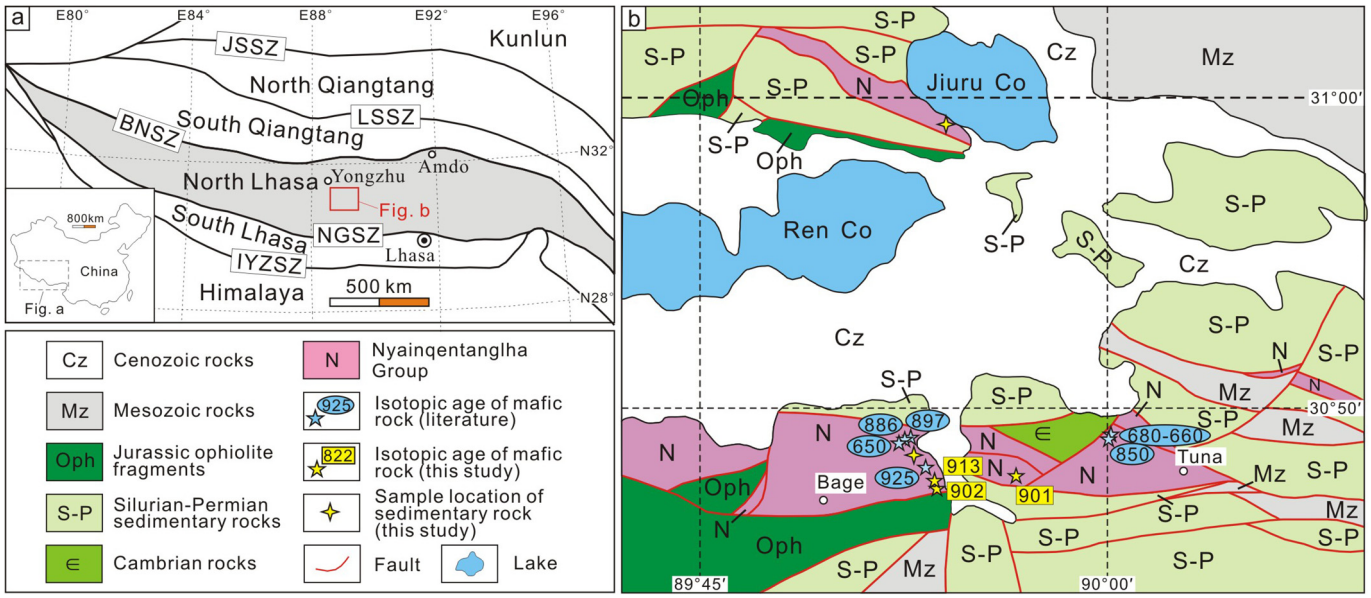

Fig. 1. (a) Tectonic framework of the Tibetan Plateau. (b) Simplified geological map of the Tuna area in the North Lhasa Terrane, Tibet. JSSZ = Jinsha suture zone; LSSZ = Longmu Co–Shuanghu suture zone; BNSZ = Bangong–Nujiang suture zone; NGSZ = North Gangdese suture zone; IYZSZ = Indus–Yarlung Zangbo suture zone. Age data sources: 925 Ma, Hu et al., 2016; 897, 886, and 650 Ma, Zhang et al., 2012; 850 and 680–660 Ma, Dong et al., 2011.

Precambrian origin and evolution of the North Lhasa Terrane. In this paper, we report the first evidence for coeval sedimentation associated with these early Neoproterozoic mafic rocks, and detrital zircon age data are used to constrain the Precambrian origin of the North Lhasa Terrane. We also report new zircon U—Pb ages, whole-rock major and trace element data, and Sr–Nd–Hf isotopic data for the early Neoproterozoic mafic meta-igneous rocks. These data are used to constrain the petrogenesis and tectonic setting of the mafic rocks, along with the Precambrian geodynamic evolution of the North Lhasa Terrane.

2. Geological background and sample descriptions

The Lhasa Terrane is located in the central Tibetan Plateau and bounded by the Bangong–Nujiang suture zone to the north and the Indus–Yarlung Zangbo suture zone to the south (Yin and Harrison, 2000). This terrane is divided into northern, central, and southern subterranes (e.g., Zhu et al., 2011b, 2013). Moreover, based on the presence of ophiolitic, arc, and eclogitic rocks in the Sumdo area, Yang et al. (2009) and Chen et al. (2009) suggested that the Lhasa Terrane comprises two separate crustal fragments: the North and South Lhasa terranes (Fig. 1a). The North Lhasa Terrane includes the central and northern subterranes. In this paper, we adopt the second classification scheme because: (1) the Shiquan River–Nam Tso mélange zone, which separates the northern and central subterranes, is considered to be a relatively short-lived Jurassic back-arc basin (e.g., Xu et al., 2014); and (2) recent studies have suggested that the ages and petrogenesis of the Precambrian rocks in the central Lhasa subterrane are different to those of the southern Lhasa subterrane, but are similar to those of the Amdo rocks (Fig. 1a) in the northern part of the Lhasa Terrane (Hu et al., 2018c).

Previous studies have shown that the North Lhasa Terrane is a microcontinent with Precambrian basement rocks (Dong et al., 2011; Hu et al., 2016; Zhang et al., 2012) covered by Paleozoic–Mesozoic sedimentary and volcanic rocks. The Nyainqentanglha Group represents the Precambrian basement of the North Lhasa Terrane (Zhang et al., 2012) and comprises a series of tectonic slices of variable size, including paragneisses, orthogneisses, and mafic–silicic intrusions (Hu et al., 2016). Recent studies have shown that most of these rocks have experienced greenschist-facies metamorphism, whereas others were subjected to amphibolite- or even granulite-facies metamorphism (Dong et al., 2011; Zhang et al., 2012, 2013). Zhang et al. (2012) described middle Neoproterozoic high-pressure granulites in the Tuna area (Fig. 1b) with a peak metamorphic age of ca. 650 Ma and that record a paleogeothermal gradient of ~14 °C/km, which were interpreted to have formed in a collisional setting. Slightly older (ca. 680–660 Ma; Dong et al., 2011) amphibolite-facies metamorphism also occurred in this area.

Hu et al. (2016) reported early Neoproterozoic (ca. 925 Ma) N-MORB-type mafic rocks in the Tuna area. This age is broadly consistent with those of the protoliths of the middle Neoproterozoic granulites (ca. 897 and 886 Ma, Zhang et al., 2012). Recently, ca. 850 Ma MORB-like (Dong et al., 2011) and ca. 822–806 Ma back-arc (Hu et al., 2018b) igneous rocks were also discovered in this area. To the northwest and in the Yongzhu area (Fig. 1a), granitoids (ca. 660 Ma) and island arc calc-alkaline basaltic rocks (ca. 742 Ma) are present. Middle Neoproterozoic metamorphism (ca. 666 Ma) has overprinted the rocks in this region (Zhang et al., 2013).

The geology of the Tuna area includes the Nyainqentanglha Group; Cambrian volcanic and sedimentary sequences; Devonian, Permian, and Jurassic sedimentary sequences; Cretaceous sedimentary and volcanic rocks; Jurassic ophiolite fragments; and Cenozoic sediments (Fig. 1b). The distribution of the Nyainqentanglha Group is controlled by several faults. In this contribution, we focus on the early Neoproterozoic amphibolites (Fig. 2c) and quartzites (Fig. 2e) in the Nyainqentanglha Group. The amphibolites can be subdivided into two groups based on their field occurrence. The group 1 amphibolites have variable sizes (5–20 m wide and 5–50 m long) and are faulted against other rocks in the Nyainqentanglha Group (Fig. 2a). The group 2 amphibolites are interbedded with quartzites (Fig. 2b). The amphibolites of both groups share similar petrological characteristics and the main minerals are hornblende (50–60 vol%) and plagioclase (45–50 vol%), with minor zircon, magnetite, and biotite (<5 vol%) (Fig. 2d). Fragmentation is observed at the margins of plagioclase and hornblende grains. Plagioclase grains have been subjected to various degrees of saussuritization and sericitization. The quartzites associated with the amphibolites consist almost entirely of quartz (Fig. 2f).

3. Analytical methods

Zircons were separated at the Special Laboratory of the Geological Team of Hebei Province, Langfang, China, by conventional heavy liquid and magnetic techniques. Insufficient zircons for U—Pb dating were

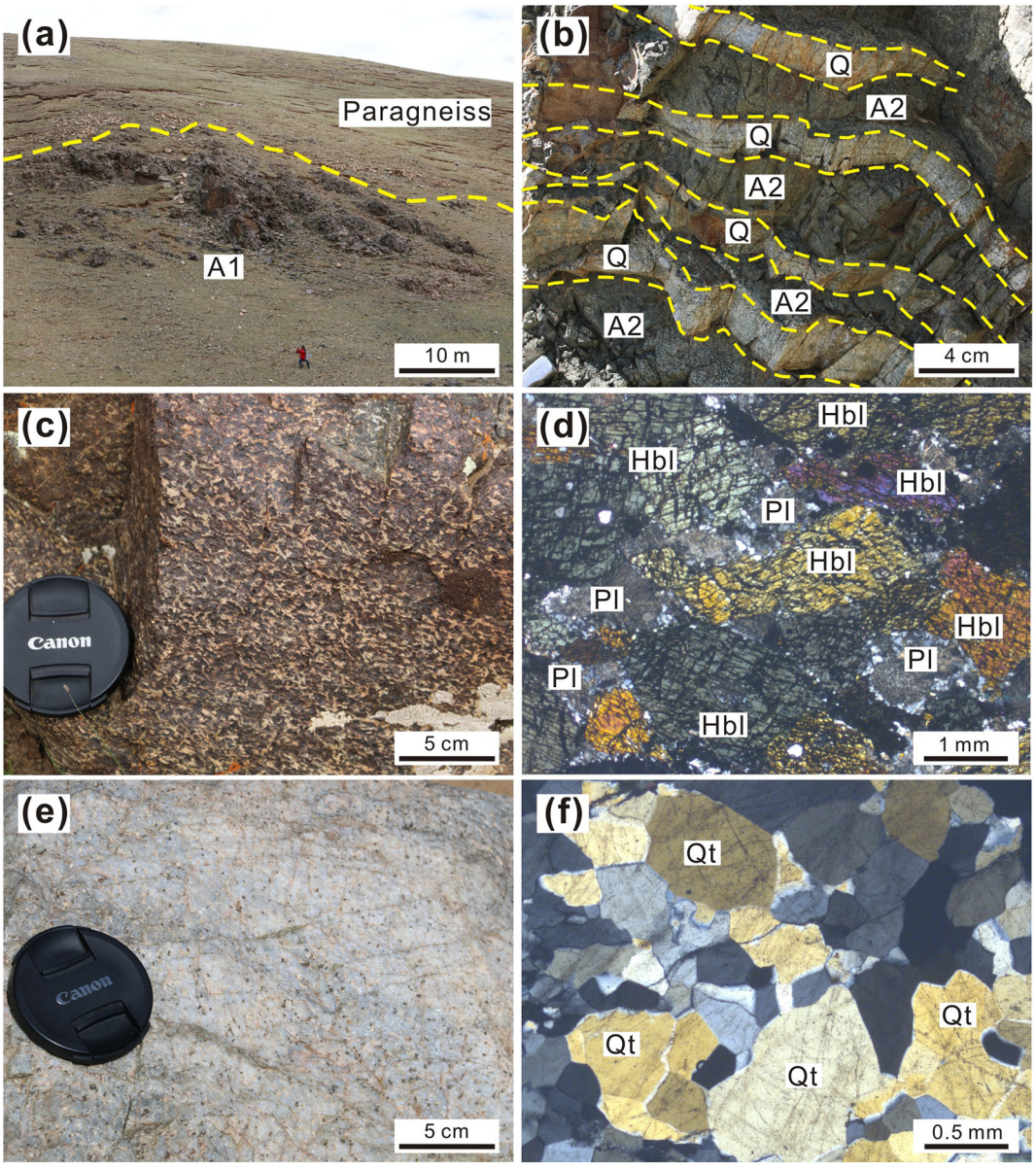

Fig. 2. Photographs and photomicrographs of the early Neoproterozoic mafic and sedimentary rocks of the North Lhasa Terrane, Tibet. A1 = Group 1 amphibolite; A2 = Group 2 amphibolite; Q = Quartzite; Hbl = hornblende; Pl = plagioclase; Qt = quartz.

obtained from the group 2 amphibolites, but enough zircons were obtained from the quartzites and group 1 amphibolites. Cathodoluminescence (CL) images were taken using a HITACHI S-3000 N scanning electron microscope fitted with a Gatan Chroma CL imaging system at the Institute of Geology, Chinese Academy of Geological Sciences, Beijing, China.

Two samples of quartzite (15 T059 and 15 T072) and three of group 1 amphibolite (16 T243, 17 T114, and 17 T138) were selected for zircon U—Pb dating at Beijing Createch Test Technology, China (Appendix A). The analyses were performed by laser ablation–inductively coupled plasma–mass spectrometry (LA–ICP–MS). Laser sampling was conducted using an ESI NWR 193 nm laser ablation system, and an AnlyitikJena PQMS Elite ICP–MS instrument was used to acquire ion signal intensities. The analyses were carried out with laser beam diameters of 25 or 20 μm, a repetition rate of 10 Hz, and an energy of 4 J/cm^2. Offline raw data selection, integration of background and analyte signals, and time-drift correction and quantitative calibration were performed by ICPMSDataCal. The age calculations and concordia diagrams were made with Isoplot/Ex ver. 3.0. During the course of this study, the mean $^{206}Pb/^{238}U$ age obtained for the zircon standard GJ-1 was 600.3 ± 1.8 Ma (2σ; n = 40), which is consistent with reported or recommended values (Jackson et al., 2004).

Hf isotopic analyses were performed at the same sites or in the same age domains (identified by CL images) as used for U—Pb dating analyses (Appendix B). The analyses were undertaken using a Geolas-193 laser ablation microprobe coupled to a Neptune multi-collector ICP–MS at the Institute of Geology and Geophysics, Chinese Academy of Sciences, Beijing, China. The ablation time was ~26 s for each measurement. The laser beam was operated at a diameter of ~50 μm, repetition rate of 8 Hz, and beam energy of 15 J/cm^2. The zircon standard Mud Tank was analyzed to evaluate accuracy and precision. During the period of analysis, a mean $^{176}Hf/^{177}Hf$ ratio of 0.282506 ± 21 (2σ; n = 40) was obtained for the Mud Tank standard, which is consistent with the values obtained by Woodhead and Hergt (2005).

We also selected 43 relatively fresh samples or the central parts of samples for whole-rock geochemical analyses (Appendix C), which were performed at the National Research Center for Geoanalysis, Beijing, China. The major elements were determined by X-ray fluorescence (XRF model PW 4400), with analytical uncertainties ranging from 1% to 3%. Loss on ignition was obtained by heating ~1 g of sample powder at

Table 1
Whole-rock Sr—Nd isotopic compositions of early Neoproterozoic mafic meta-igneous rocks of the North Lhasa Terrane, Tibet.

Sample	Age (Ma)	[Rb] (ppm)	[Sr] (ppm)	$^{87}Rb/^{86}Sr$	$^{87}Sr/^{86}Sr$	±2σ(m)	I_{Sr}	[Sm] (ppm)	[Nd] (ppm)	$^{147}Sm/^{144}Nd$	$^{143}Nd/^{144}Nd$	±2σ(m)	$\varepsilon_{Nd}(0)$	$\varepsilon_{Nd}(t)$	$f_{Sm/Nd}$
Group-1															
16T242	900	20.2	174	0.337	0.713100	16	0.709	4.40	12.6	0.2118	0.513016	5	7.4	5.6	0.08
16T253	900	7.00	182	0.111	0.708581	13	0.707	5.51	15.0	0.2224	0.513076	12	8.5	5.6	0.13
Group-2															
15T117	900	9.79	181	0.156	0.707276	10	0.705	5.53	15.3	0.2189	0.513056	5	8.2	5.6	0.11
15T119	900	12.5	157	0.231	0.707018	14	0.704	5.56	15.4	0.2190	0.513050	9	8.0	5.5	0.11
16T237	900	15.7	150	0.303	0.714859	15	0.711	4.59	12.5	0.2214	0.513092	10	8.9	6.0	0.13

980 °C for 30 min. The trace elements were analyzed with an Agilent 7500ce ICP–MS. Data quality was monitored by analyses of reference materials AGV-2 and GSR-3 (Govindaraju, 1994; Wang et al., 2003). The accuracy was generally better than 10% for elements with concentrations of <10 ppm and ~5% for elements with concentrations of >10 ppm (Appendix D).

Subsequently, five whole-rock samples were selected for Sr—Nd isotopic analysis using a Finnigan MAT-262 mass spectrometer at the Institute of Geology, Chinese Academy of Geological Sciences, Beijing, China (Table 1). Blanks for the whole chemical procedure were ~10^{-11} g for Sm and Nd, and ~10^{-10} g for Rb and Sr. $^{87}Sr/^{86}Sr$ ratios were corrected for instrumental mass fractionation relative to $^{88}Sr/^{86}Sr = 8.37521$. The average $^{87}Sr/^{86}Sr$ ratio determined for the NBS987 standard was 0.710247 ± 12 ($2\sigma_m$). $^{143}Nd/^{144}Nd$ ratios were corrected for instrumental mass fractionation relative to $^{146}Nd/^{144}Nd = 0.7219$ and are reported relative to the JMC Nd_2O_3 standard with a $^{143}Nd/^{144}Nd$ ratio of 0.511230 ± 10 ($2\sigma_m$). The decay constants (λ) used are 1.42 × 10^{-11} a^{-1} for ^{87}Rb and 6.54 × 10^{-12} a^{-1} for ^{147}Sm. $\varepsilon_{Nd}(t)$ values were calculated on the basis of the following present-day reference values for the chondritic uniform reservoir (CHUR): $(^{143}Nd/^{144}Nd)_{CHUR} = 0.512638$ and $(^{147}Sm/^{144}Nd)_{CHUR} = 0.1967$.

4. Results

4.1. Zircon U—Pb geochronology

The zircon grains from the group 1 amphibolite samples (16 T243, 17 T114, and 17 T138) have lengths of 50 to 150 μm and length:width ratios of 2:1 to 1:1 (Fig. 3). Most zircon grains from samples 16 T243 and 17 T138 are characterized by igneous cores surrounded by CL-light metamorphic rims (5–50 μm). The igneous cores show patchy and weak oscillatory zoning. The analyses of the igneous cores are concordant and yielded weighted-mean $^{206}Pb/^{238}U$ ages of 902 ± 6 Ma (n = 15; Fig. 4a) and 901 ± 9 Ma (n = 13; Fig. 4c). Th/U ratios (0.27–3.58) are >0.1, indicating a magmatic origin (Hoskin and Schaltegger, 2003). Two analyses (spots 14 and 17) on metamorphic zircon rims in sample 17 T138 yield low Th/U ratios (0.04 and 0.01) and their $^{206}Pb/^{238}U$ ages (866 and 797 Ma) may represent the timing of metamorphism after magmatic crystallization (Hoskin and Schaltegger, 2003). The zircon grains from sample 17 T114 show weak oscillatory zoning and no metamorphic rims were observed, and they yield a weighted-mean $^{206}Pb/^{238}U$ age of 903 ± 7 Ma (n = 16; Fig. 4b). They also have high Th/U ratios (0.61–7.77) which are comparable with those of magmatic zircons (Hoskin and Schaltegger, 2003).

The zircon grains from the quartzite samples (15 T059 and 15 T072) are mostly transparent and colorless, with diameters of 100–200 μm. Most zircon grains from sample 15 T059 are partly rounded and exhibit regular oscillatory zoning (Fig. 3). The zircon grains from sample 15 T072 have detrital cores with oscillatory and banded zoning, and are mainly surrounded by unzoned metamorphic rims (5–30 μm thick) (Fig. 3). In total, 181 spots were analyzed and most of the data are concordant, with 6 analyses showing >10% discordance. In this paper, ages older than 1.0 Ga are $^{207}Pb/^{206}Pb$ ages, whereas ages younger than 1.0 Ga are $^{206}Pb/^{238}U$ ages. A total of 169 concordant analyses on zircons of sample 15 T059 and detrital zircon cores of sample 15 T072 yield highly variable U—Pb ages of 2748–931 Ma and are characterized by a main age population of 1200–1000 Ma (Fig. 5). Their

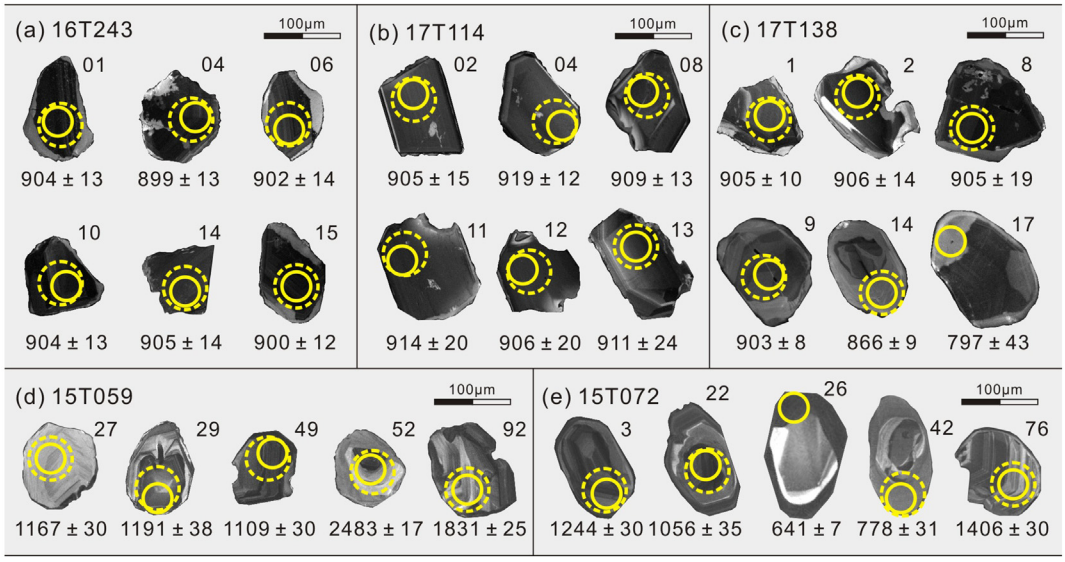

Fig. 3. Cathodoluminescence images of representative zircon grains from the early Neoproterozoic mafic and sedimentary rocks in the North Lhasa Terrane, Tibet. Solid and dashed circles indicate the locations of U—Pb dating and Hf isotopic analyses, respectively.

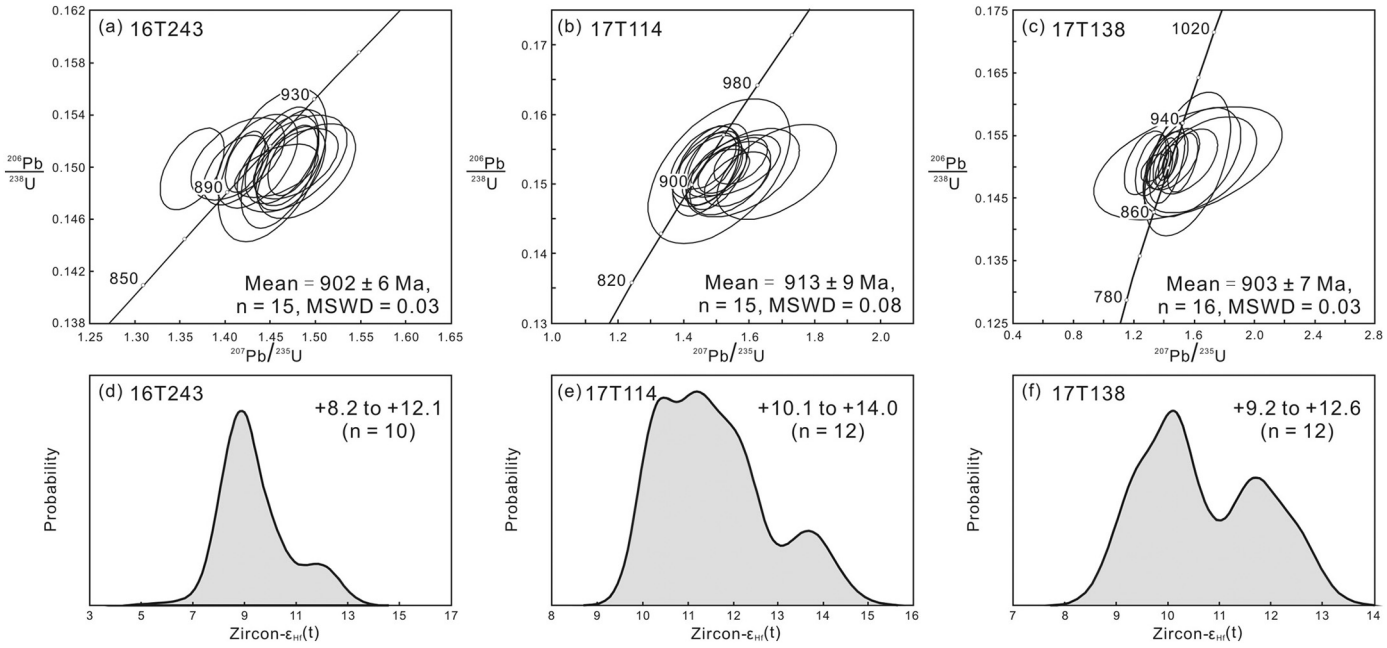

Fig. 4. (a–c) Zircon U—Pb concordia diagrams and (d–f) histograms of zircon $\varepsilon_{Hf}(t)$ values for early Neoproterozoic mafic rocks from the North Lhasa Terrane, Tibet.

relatively high Th/U ratios (0.12–2.90; i.e., >0.1) indicate a magmatic origin (Hoskin and Schaltegger, 2003). Six analyses of metamorphic zircon rims in sample 15 T072 yield lower Th/U ratios (0.02–0.11) and younger ages of 869–641 Ma, constraining the timing of metamorphism (Hoskin and Schaltegger, 2003).

4.2. Zircon Hf and whole-rock Sr—Nd isotope data

Thirty-four Hf isotopic analyses of the zircons from the group 1 amphibolites yielded high positive $\varepsilon_{Hf}(t)$ values (+7.2 to +14.0; Fig. 4d–f). The ca. 1200–1000 Ma zircons from the quartzites display variable $\varepsilon_{Hf}(t)$ values (−14.7 to +12.7) (Fig. 6a) and crustal model ages (T^{C}_{DM} = 1.3–2.8 Ga). The amphibolites of both groups share similar whole-rock Sr—Nd isotopic compositions, with initial $^{87}Sr/^{86}Sr$ ratios (I_{Sr}) of 0.704 to 0.711 and $\varepsilon_{Nd}(t)$ values of +5.5 to +6.0 (Fig. 7d).

4.3. Whole-rock major and trace element data

The group 1 amphibolite samples have undergone metamorphism, which is evident from the presence of metamorphic zircon rims (Fig. 3). Although the amphibolites of both groups have relatively low loss-on-ignition values (0.43–1.94 wt%), saussuritization and sericitization were observed in thin section. These metamorphic and alteration processes may have modified the concentrations of mobile elements (e.g., Na, K, Rb, Ba, Sr, and Pb) (e.g., Zhai et al., 2013), as indicated by the variable contents of mobile elements in the amphibolites (e.g., Rb = 3.23–31.2 ppm, Pb = 0.44–3.88 ppm, and Ba = 23.9–142 ppm). Therefore, we focus mainly on the abundances of immobile (e.g., rare earth and high-field-strength elements) and transition (e.g., V, Sc, Ni, Cr, and Fe) elements, their corresponding ratios, and whole-rock Nd and zircon Hf isotopic compositions in classifying these rocks and investigating their petrogenesis.

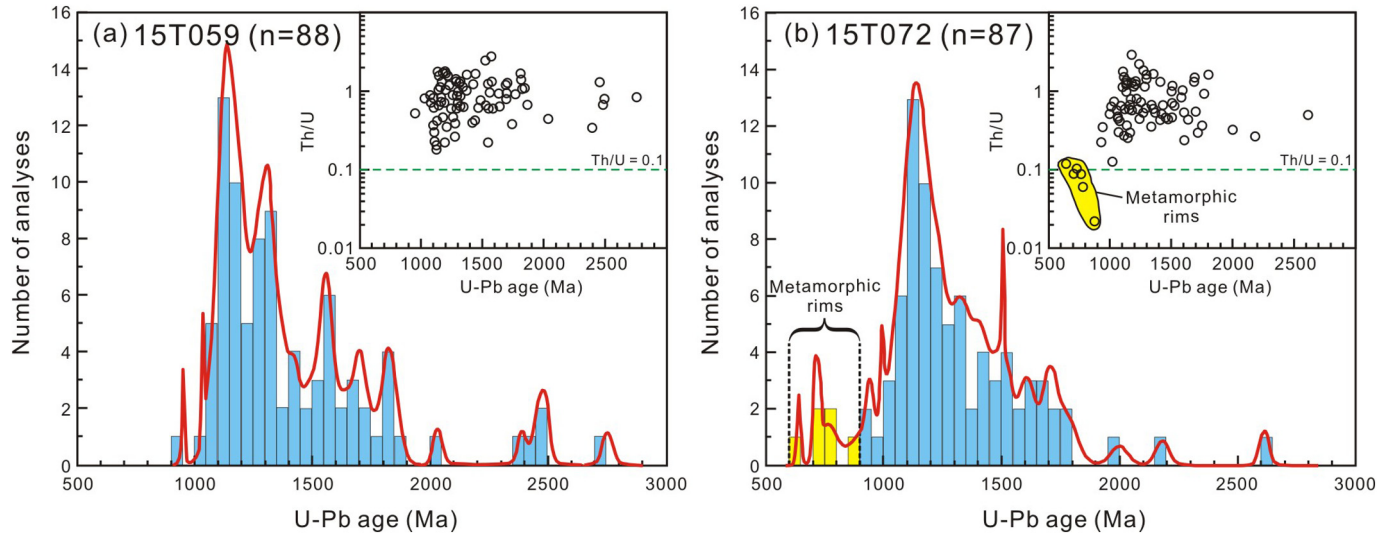

Fig. 5. Age distributions of detrital zircons from early Neoproterozoic metasedimentary rocks of the North Lhasa Terrane, Tibet.

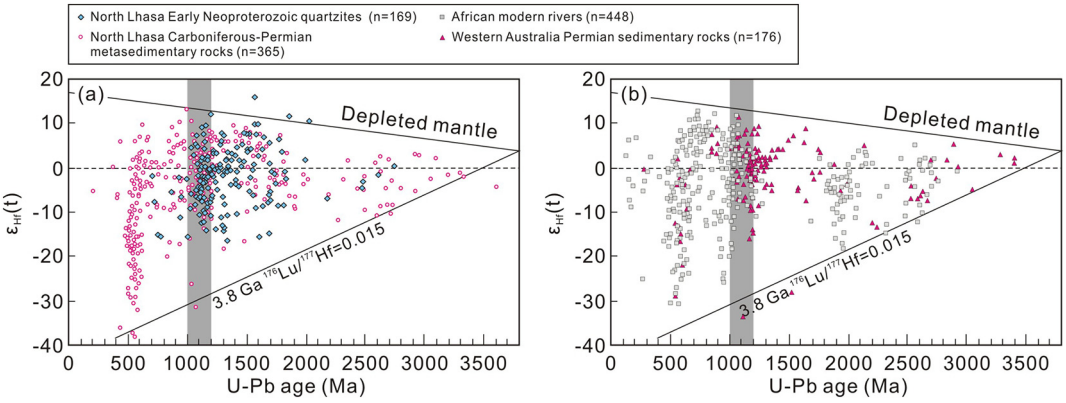

Fig. 6. $\varepsilon_{Hf}(t)$ vs. U—Pb age diagrams for detrital zircons from metasedimentary rocks of this and previous studies. Data sources: Carboniferous–Permian sedimentary rocks of the North Lhasa terrane (Zhu et al., 2011a); African modern rivers (Iizuka et al., 2013); and Permian sedimentary rocks of the Western Australia (Clark et al., 2000).

The amphibolites of both groups share similar geochemical characteristics (Figs 7–9). They both have variable SiO_2 (42.72–50.53 wt%; hereafter, all whole-rock major element data have been normalized to an anhydrous basis), TiO_2 (1.16–4.34 wt%), Al_2O_3 (11.49–17.66 wt%), and Fe_2O_3t (8.95–20.96 wt%) contents, and $Mg^{\#}$ (= Mg/[Mg + Fe_T]) values (39–66). Data for the amphibolites fall in the field of sub-alkaline basalts when plotted in the SiO_2 vs. Zr/Ti diagram (Fig. 7a). A clear positive correlation between TiO_2 contents and FeOt/MgO ratios is evident in Fig. 7b, suggesting a tholeiitic affinity. Variation diagrams (Fig. 8) show a positive correlation in $Mg^{\#}$ vs. Al_2O_3 and negative correlations in $Mg^{\#}$ vs. Fe_2O_3t, TiO_2, Zr, and V diagrams. Rare earth and high-field-strength element data are generally comparable with those of normal mid-ocean ridge basalt (N-MORB) (Fig. 9a and b). No significant Eu anomalies are observed (Eu/Eu* = 0.80–1.05). Primitive-mantle-normalized trace element patterns show variable contents of Th, Zr, Hf, and Ti (Fig. 9b).

5. Discussion

5.1. Early Neoproterozoic (ca. 900 Ma) sedimentation and mafic magmatism in the North Lhasa Terrane

The concordant analyses on zircons of sample 17 T114 and igneous zircon cores of samples 16 T243 and 17 T138 have high Th/U ratios (>0.1) and yield highly consistent U—Pb ages of ca. 913–902 Ma, indicating that these ages can be interpreted as the crystallization ages of the protoliths of group 1 amphibolites. This interpretation seems not to be supported by the fragmentary shapes of these zircons or zircon igneous cores (Fig. 3). Generally, the velocity of crystallization appears to be the major controlling factor of the elongation ratio for zircon. Skeletal zircon crystals are the most extreme form of rapid growth and are common in co-magmatic zircons from mafic rocks (Corfu et al., 2003). However, in some gabbroic magmas, Zr saturation is only reached late in the

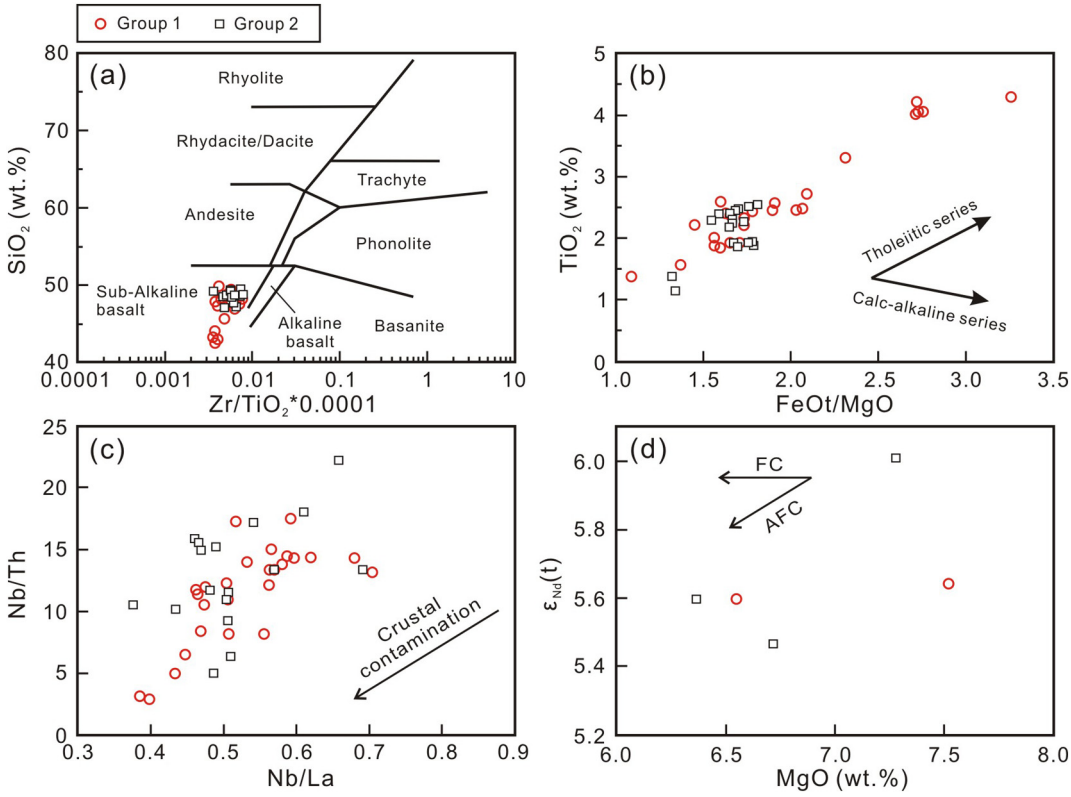

Fig. 7. (a) SiO_2 vs. Zr/Ti (Winchester and Floyd, 1977), (b) TiO_2 vs. FeOt/MgO (Miyashiro, 1974), (c) Nb/Th vs. Nb/La (Li et al., 2006), and (d) $\varepsilon_{Nd}(t)$ vs. MgO (Li et al., 2006) diagrams for early Neoproterozoic amphibolites from the North Lhasa Terrane, Tibet. FC = fractional crystallization; AFC = assimilation and fractional crystallization.

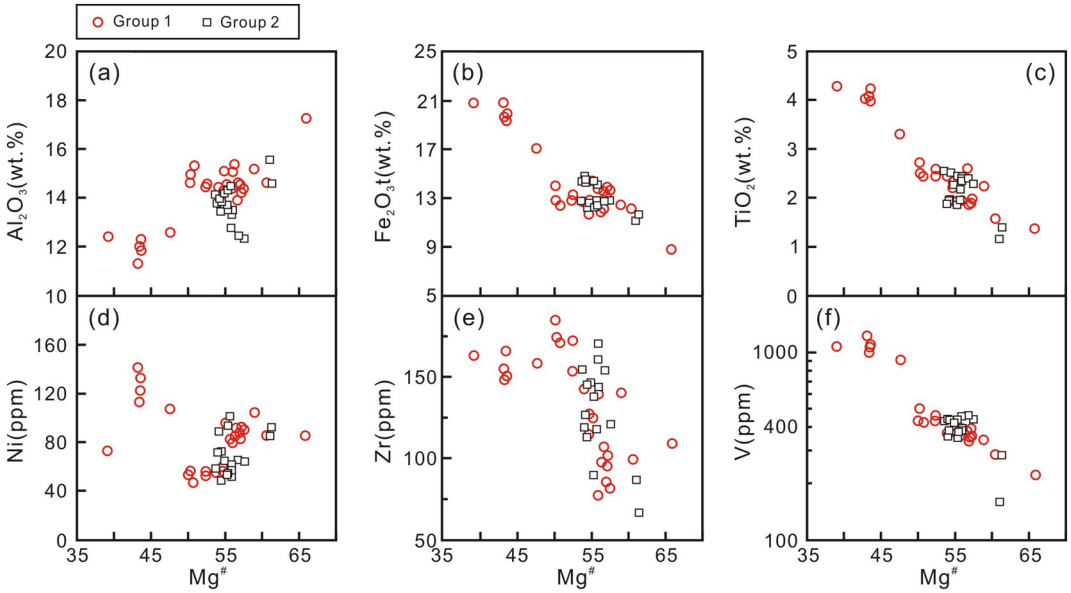

Fig. 8. Plots of major and trace elements versus $Mg^{\#}$ for early Neoproterozoic amphibolites from the North Lhasa Terrane, Tibet.

crystallization history, either because of very low Zr contents, or high Zr solubility or both (Corfu et al., 2003). In such case, zircon is interstitial mineral and may be fragmentary. This is probably the case in this study as suggested by the negative Zr–$Mg^{\#}$ correlation of the group 1 amphibolites (Fig. 8e).

Zhang et al. (2012) reported the presence of high-pressure granulites in the North Lhasa Terrane with middle (ca. 650 Ma) and early (ca. 897 and 886 Ma) Neoproterozoic peak metamorphic and protolith ages, respectively. Subsequently, secondary ion mass spectrometry (SIMS) zircon U—Pb dating of mafic rocks in the Nyainqentanglha Group yielded concordant ages of ca. 925 Ma (Hu et al., 2016). In this contribution, we further reveal the presence of early Neoproterozoic mafic magmatism in the North Lhasa Terrane by LA–ICP–MS zircon U—Pb dating. The protoliths of group 1 amphibolites were probably formed at ca. 913–902 Ma. Although no ages were obtained for the group 2 amphibolites, they are expected to be coeval with the group 1 amphibolites, given the similar geochemical (Figs 7–9) and isotopic (Fig. 7d) characteristics of the two groups. Moreover, the depositional age of the quartzites is between ca. 931 (youngest core of detrital igneous zircon) and 869 Ma (oldest metamorphic zircon rim). Therefore, we suggest that the protolith ages of the amphibolites and quartzites are both ca. 900 Ma.

5.2. Petrogenesis of the mafic rocks

Mafic rocks emplaced in a continental setting may undergo crustal contamination during ascent and/or residence within the continental crust (e.g., Li et al., 2006). All the amphibolites of the present study display a positive correlation between Nb/La and Nb/Th ratios (Fig. 7c), indicating crustal assimilation during magmatic evolution. The broad positive correlation between MgO and $\varepsilon_{Nd}(t)$ in Fig. 7d also suggests the presence of assimilation and fractional crystallization (AFC) processes.

Fractional crystallization plays an important role in the petrogenesis of basaltic rocks and modifies elemental concentrations. Although $Mg^{\#}$ values may be modified during AFC processes, some significative evolution trends are recognized in the plots of major and trace elements versus $Mg^{\#}$ (Fig. 8). The present samples exhibit a positive correlation between Al_2O_3 and $Mg^{\#}$ (Fig. 8a), which may reflect plagioclase fractionation. The variable Ti contents (Fig. 9b) and negative correlations between $Mg^{\#}$ and Fe_2O_3t (Fig. 8b), TiO_2 (Fig. 8c), and V (Fig. 8f) possibly indicate late-stage fractionation of Fe—Ti oxides. As noted above, the negative correlation between Zr and $Mg^{\#}$ (Fig. 8e) is consistent with zircon crystallization in the late stages of magma crystallization. Of note, the amphibolites have a range of $Mg^{\#}$ values (39 to 66) that indicate the fractional crystallization of olivine and pyroxene, but there is no clear correlation in the Ni vs. $Mg^{\#}$ diagram (Fig. 8d). This discrepancy may be attributed to the modification of $Mg^{\#}$ values during AFC processes.

Generally, magmas derived from N-MORB-type mantle sources are depleted in light rare-earth elements (LREE) while crust and the other mantle (e.g., *E*-MORB) sources produce melts with LREE enrichment (Rudnick and Fountain, 1995; Sun and McDonough, 1989). The amphibolites are characterized by LREE-depleted patterns (Fig. 9a). Because LREE contents were probably elevated during AFC processes, the primary magma of these amphibolites should have even lower LREE contents. This chemical feature suggests a N-MORB-type mantle source. Although reduced during the AFC processes, the positive zircon $\varepsilon_{Hf}(t)$ (+7.2 to +14.0) and whole-rock $\varepsilon_{Nd}(t)$ (+5.5 to +6.0) values are still as high as those of N-MORB-type rocks (Wu et al., 2006; Zhai et al., 2013). Moreover, the samples have lower Zr/Hf ratios (28.3–36.0) than the chondritic value (36.3). This feature has been interpreted by Weyer et al. (2003) to indicate a highly depleted mantle source.

Rare earth element contents of mafic rocks can constrain the nature and depth of their mantle source (Chen et al., 2017; D'Orazio et al., 2001; Wang et al., 2018). The amphibolite samples show pronounced depletions in light rare earth elements (Fig. 9a), with low $(La/Yb)_N$ ratios of 0.45–1.55, suggesting that garnet was not present in the mantle source. Moreover, a $(Sm/Yb)_N$ vs. $(La/Sm)_N$ diagram indicates that these samples could have been generated by >20% partial melting of spinel lherzolite (D'Orazio et al., 2001) (Fig. 9c). Considering the La enrichment during AFC processes, we suggest that the degree of partial melting may be even higher.

5.3. Tectonic setting

N-MORB-like rocks were originally interpreted to represent basaltic rocks formed in a normal mid-ocean ridge setting (e.g., Sun and Mcdonough, 1989). Subsequently, N-MORB-type melts have been widely reported in arc-related settings, such as back-arc and fore-arc basins (e.g., Dilek and Furnes, 2011; Zhai et al., 2013). Several recent studies have suggested that N-MORB-like rocks can also be produced in a continental rift setting (e.g., Chen et al., 2017; Pang et al., 2016).

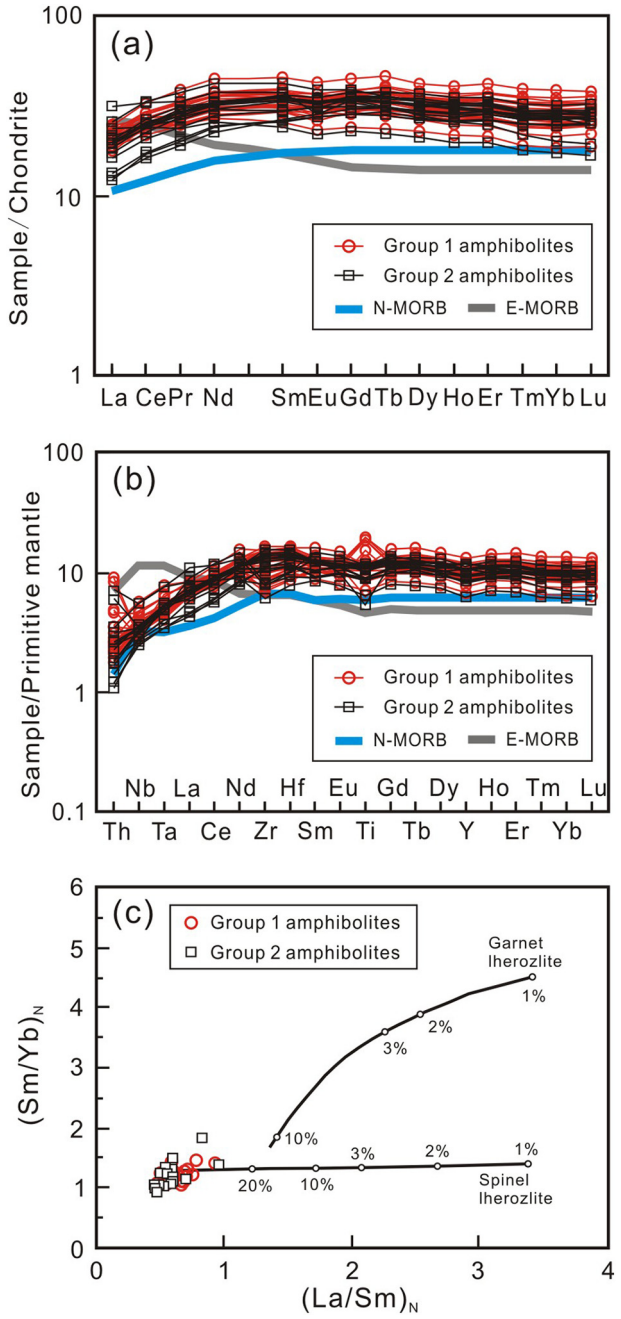

Fig. 9. (a) Chondrite-normalized rare earth element patterns, (b) primitive-mantle-normalized trace element patterns, and (c) $(Sm/Yb)_N$ vs. $(La/Sm)_N$ diagram for early Neoproterozoic amphibolites from the North Lhasa Terrane, Tibet. Values for chondrite, primitive mantle, N-MORB (normal mid-ocean ridge basalt), and *E*-MORB (enriched mid-ocean ridge basalt) are from Sun and McDonough (1989). Batch melting trends for spinel and garnet lherzolite are from D'Orazio et al. (2001). Numbers along the curves represent the degree of partial melting.

Sediments (i.e., cherts) at normal mid-ocean ridge settings should not contain old detrital zircons, which is contrary to those observed in the quartzites interbedded with the amphibolites in the present study (Fig. 5), and so we discount this possibility. Moreover, sediments at convergent plate margins are characterized by a large proportion of detrital zircon ages close to their depositional age (Cawood et al., 2012), which contrasts with the rare 1000–900 Ma detrital zircon ages in the quartzites (Fig. 5).

Rifting is considered to be the prelude to continent break-up and the formation of incipient oceanic basins, and N-MORB-like magma is not produced until the late stages of rifting when embryonic oceanic crust forms (Chen et al., 2017; Fitton, 2007). A typical example of this is the early Permian mantle plume that led to the break-up of the northern margin of Gondwana and the opening of several Tethyan oceanic basins (Chauvet et al., 2008; Chen et al., 2017; Zhu et al., 2010). In this case, the early rifting stage (ca. 301–279 Ma) produced basaltic rocks with OIB-like geochemical features (Chauvet et al., 2008; Zhu et al., 2010), whereas crustally contaminated N-MORB-like rocks were generated during the late stage of rifting (ca. 278 Ma) (Chen et al., 2017). Therefore, the early Neoproterozoic sediments and mafic rocks of our study probably represent the late-stage products of a rift. To our knowledge, the quartzites mark the oldest rift sediments in the North Lhasa Terrane, as well as within the Tibetan Plateau.

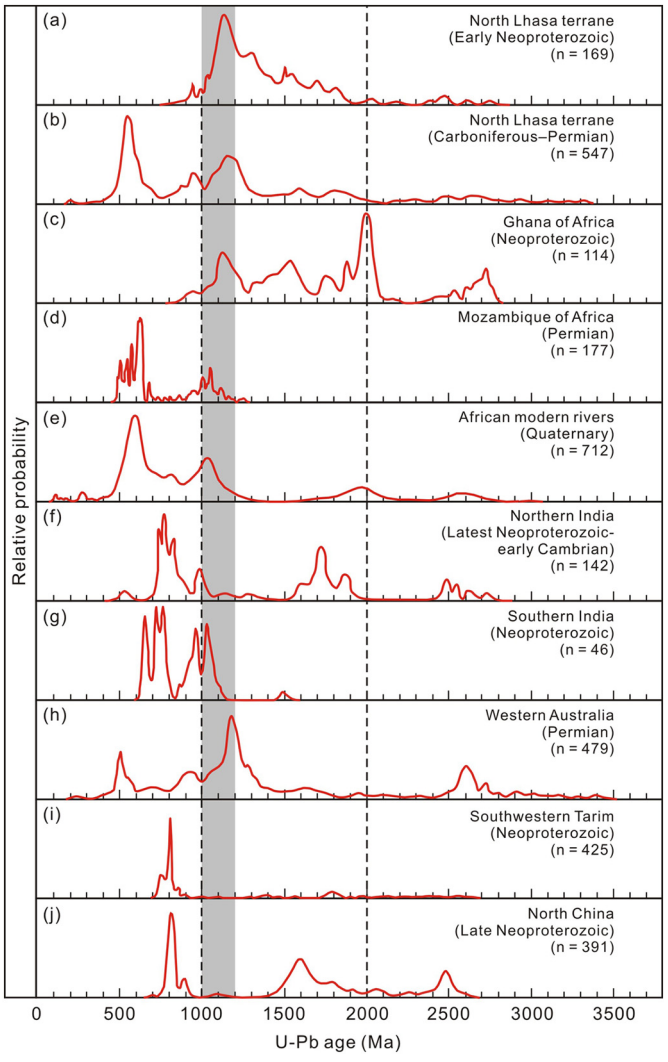

Fig. 10. Summary of detrital zircon ages in sedimentary rocks from this and previous studies. $^{207}Pb/^{206}Pb$ ages were used for zircons with ages of >1000 Ma and $^{206}Pb/^{238}U$ ages for younger zircons. Results described in this study exclude analyses with >10% discordance. Data sources: Carboniferous–Permian sedimentary rocks of the North Lhasa terrane (Zhu et al., 2011a); Neoproterozoic sedimentary rocks of the Ghana of Africa (Kalsbeek et al., 2008); Permian sedimentary rocks of the Mozambique of Africa (Bicca et al., 2018); African modern rivers (Iizuka et al., 2013); Latest Neoproterozoic–early Cambrian sedimentary rocks of the Northern India (McKenzie et al., 2011); Neoproterozoic sedimentary rocks of the Southern India (Plavsa et al., 2014); Permian sedimentary rocks of the Western Australia (Clark et al., 2000); Neoproterozoic sedimentary rocks of the southwestern Tarim (Zhang et al., 2016); and Late Neoproterozoic sedimentary rocks of the North China (Dong et al., 2017).

5.4. Geodynamic implications

5.4.1. Early Neoproterozoic paleogeography of the North Lhasa Terrane

It is generally accepted that the North Lhasa Terrane was part of northern Gondwana; however, its precise location during the Neoproterozoic remains controversial (e.g., Gehrels et al., 2011; Hu et al., 2018a; Zhang et al., 2012; Zhu et al., 2011a). Early studies had suggested that the North Lhasa Terrane was located in northeastern India, northern Australia, or the northern EAO during the Neoproterozoic (e.g., Audley-Charles, 1984; Gehrels et al., 2011; Hu et al., 2018a; Zhang et al., 2012; Zhu et al., 2011a).

Detrital zircon dating of sedimentary rocks (and their metamorphosed equivalents) has proven to be a powerful tool for tracing their provenance and for paleogeographic reconstructions of continents (e.g., Zhu et al., 2011a). As shown in Fig. 10a, the detrital zircons from the quartzites are characterized by a distinct age population of 1200–1000 Ma and a lack of 1000–900 Ma ages. In contrast, the latest Neoproterozoic–early Cambrian metasedimentary rocks in northern India define an age population of ca. 950 Ma and contain rare 1200–1000 Ma detrital zircons (Fig. 10f; McKenzie et al., 2011). Although 1200–1000 Ma detrital zircons have been recognized from some Neoproterozoic metasedimentary rocks in southern India, they also contain a distinctive age population at 1000–900 Ma (Fig. 10g; Plavsa et al., 2014).

The 1200–1000 Ma age population has been recognized in Carboniferous–Permian sedimentary rocks in the North Lhasa Terrane (Fig. 10b) and is interpreted to be related to the Wilkes–Albany–Fraser Orogen of Western Australia (Fig. 10h) (Zhu et al., 2011a). This interpretation is supported by the similar $\varepsilon_{Hf}(t)$ values of the 1200–1000 Ma detrital zircons from the early Neoproterozoic quartzites in the North Lhasa Terrane and the Permian sedimentary rocks in the Wilkes–Albany–Fraser Orogen (Fig. 6a). However, a ca. 900 Ma rift event is absent in Western Australia, which is inconsistent with this interpretation.

The EAO is one of the largest continuous orogenic belts on Earth, extending over 6000 km, from Arabia in the north along the eastern African and western Indian margins into East Antarctica (Fritz et al., 2013; Mole et al., 2018). The northern EAO is marked by a Pacific-sized ocean basin (the Mozambique Ocean), which accumulated oceanic terranes and arcs for >400 Myr (from prior to ca. 1080 until 600 Ma; Merdith et al., 2017; Mole et al., 2018), and separated the continental components of India and Arabia–Africa (Meert, 2003). Recently, middle Neoproterozoic arc-related magmatism and metamorphism (ca. 822–660 Ma; Dong et al., 2011; Zhang et al., 2013; Hu et al., 2018b) and collision-related, high-pressure metamorphism (ca. 650 Ma; Zhang et al., 2012) have been identified in the North Lhasa Terrane, indicating an affinity to the northern EAO (Fritz et al., 2013). The Neoproterozoic metamorphism (ca. 869–641 Ma; Fig. 5b) identified in the present study is comparable to that in the EAO (Mole et al., 2018).

This affinity to the northern EAO is also supported by the temporal and spatial distribution of Ediacaran–early Paleozoic magmatism on the Gondwana supercontinent. Extensive Ediacaran–early Paleozoic Andean-type magmatism has been recognized in terranes along the proto-Tethyan margin of Gondwana. It is notable that Andean-type magmatism in the terranes from the Arabian proto-Tethyan margin (601–522 Ma) is clearly older than that of the Indian–Australian proto-Tethyan margin (512–462 Ma) (Hu et al., 2018a and references therein) (Fig. 11). Interestingly, Andean-type magmatism in the North Lhasa Terrane was prolonged (568–488 Ma) and comparable to that on both the Arabian and Indian–Australian proto-Tethyan margins (Fig. 11). This suggests that the North Lhasa Terrane was derived from the northern EAO between the Arabian and Indian–Australian continents (Hu et al., 2018a).

If the North Lhasa Terrane has an affinity to the northern EAO, then a further question arises as to whether it originated from the African or Indian side of the EAO. As discussed above, our detrital zircon age data are inconsistent with those from India (Fig. 10f and g). In contrast, the 1200–1000 Ma age population is common on the African side of the northern EAO, such as in Neoproterozoic metasedimentary rocks from Ghana (Fig. 10c; Kalsbeek et al., 2008), Permian sedimentary rocks in Mozambique (Fig. 10d; Bicca et al., 2018), and Quaternary sediments in modern African rivers (Fig. 10e; the Niger, Nile, Congo, Zambezi, and Orange rivers; Iizuka et al., 2013). The 1200–1000 Ma detrital zircons from the North Lhasa Terrane and Africa have similar ε_{Hf} (t) values (mostly between −15 and + 10; Fig. 6a and b). Although the quartzite samples contain numerous 1200–1700 Ma detrital zircons, which are absent in Quaternary sediments in modern African rivers (Fig. 10e), a coeval age population has been recognized in Neoproterozoic metasedimentary rocks from Ghana (Fig. 10c). It is noteworthy that the remarkable ca. 2000 Ma zircon U—Pb age peaks shown by detrital zircons from Ghana of Africa (Fig. 10c) and African modern rivers (Fig. 10e) are nearly absent in the detrital zircon age data of this study. This may be because the ca. 2000 Ma rocks were not extensively exposed and eroded at ca. 900 Ma or rivers did not pass through these rocks at this time. For example, Permian rocks from the Perth Basin, located next to the present-day Archean Yilgarn Craton of Western Australia, have few Archean ages (Cawood and

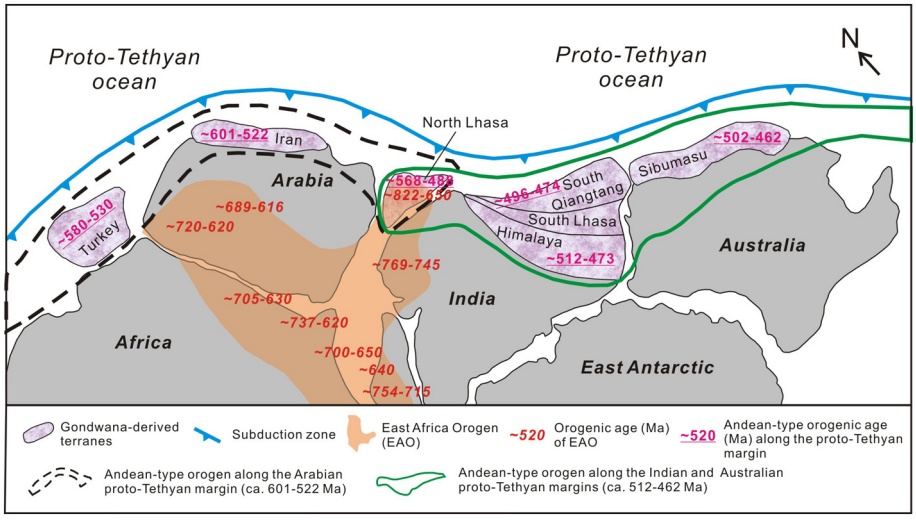

Fig. 11. Reconstruction of northern Gondwana showing the locations of continents and smaller terranes in the Ediacaran–Early Paleozoic (modified from Meert, 2003; Hu et al., 2018a). The EAO and its ages are from Meert (2003), Collins et al. (2003), Doebrich et al. (2007), Fritz et al. (2013), Lundmark et al. (2012), Dong et al. (2011), Zhang et al. (2013), Hu et al. (2018b), and Mole et al., (2018). The geochronological data for the Andean-type orogen along the proto-Tethyan margin are after Hu et al. (2018a) and references therein.

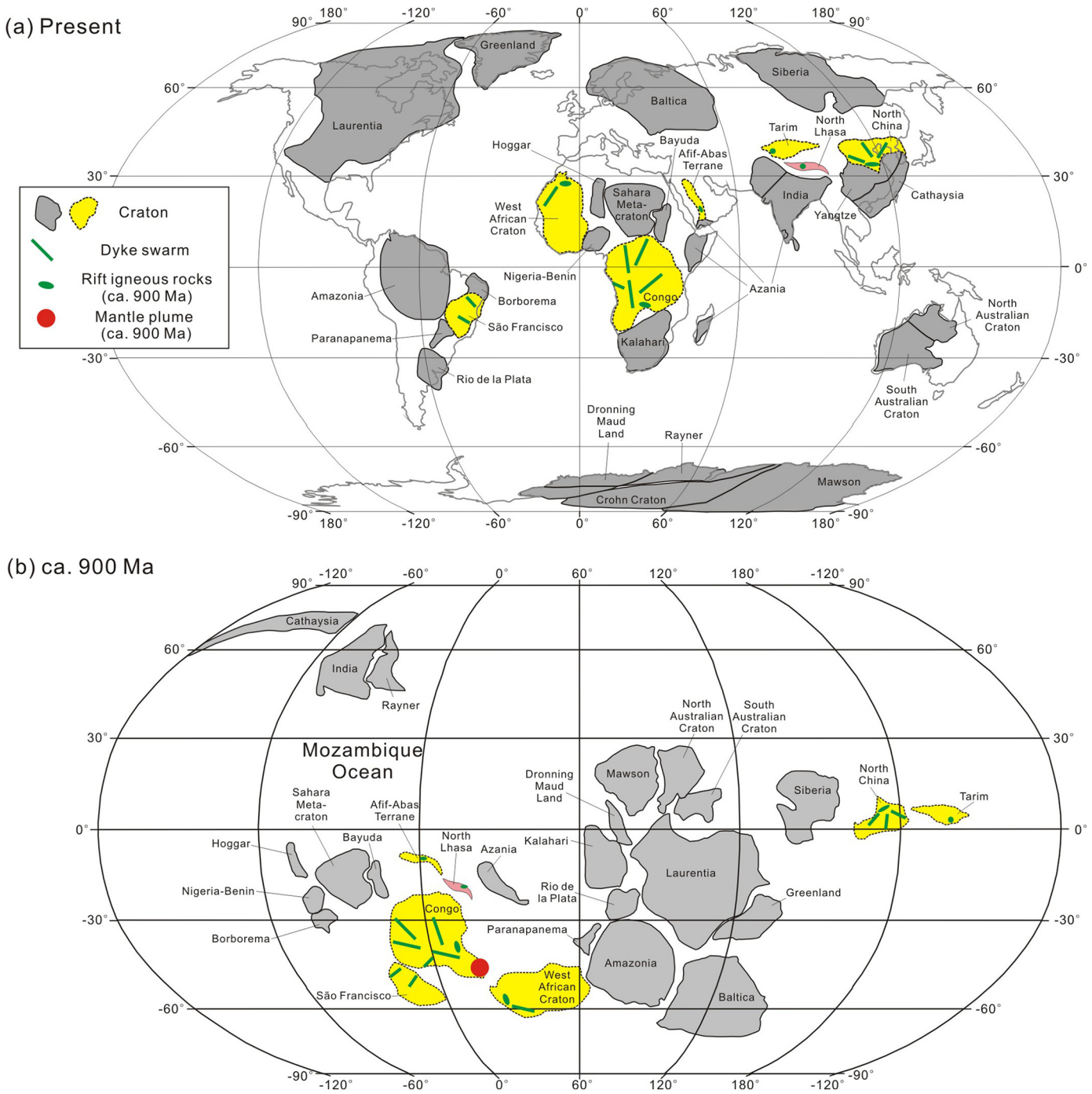

Fig. 12. (a) Present-day geographical map of the world, showing the locations of Precambrian cratons, and ca. 900 Ma dike swarms and rift-related igneous rocks (Álvaro et al., 2014; Evans et al., 2015; Peng et al., 2011a, 2011b; Stein, 2003; Wang et al., 2015). (b) Paleogeographic map at ca. 900 Ma (after Merdith et al., 2017; Wu et al., 2017).

Nemchin, 2000). Typically, absence of an age peak is not particularly diagnostic; it is the presence of ages that provides strong evidence.

The sedimentation and mafic magmatism documented in this contribution are related to an early Neoproterozoic rift. The identification of matching rift events in different regions can provide constraints on paleogeographic reconstructions. Coeval rift-related igneous rocks have been identified from the São Francisco, Congo, West African, Tarim, and North China cratons and the Afif–Abas Terrane (Fig. 12a). In the São Francisco craton, mafic dikes with baddeleyite U—Pb ages of ca. 920 Ma have been reported (Evans et al., 2015). Coeval mafic dikes, continental flood basalts, and rift-related rhyolitic volcanic rocks (ca. 924–912 Ma) are present in the Congo craton (Correa-Gomes and Oliveira, 2000; Franssen and André, 1988; Tack et al., 2001). Correa-Gomes and Oliveira (2000) correlated the dikes of the São Francisco and Congo cratons, thereby suggesting a paleogeographic link between these cratons. Early Neoproterozoic rift-related magmatism is also found at the Anti–Atlas margin of the West African Craton (Álvaro et al., 2014). The early Neoproterozoic oceanic plateaus in the Afif–Abas Terrane were related to a ca. 900 Ma mantle plume (Stein, 2003). Rift-related mafic dikes and sills were intruded into the North China Craton at ca. 925–900 Ma (Peng et al., 2011a, 2011b), and slightly younger bimodal, rift-related volcanism (ca. 900–870 Ma) occurred in the Tarim Craton (Wang et al., 2015). In a recently published full-plate global reconstruction for ca. 900 Ma (Merdith et al., 2017; Wu et al., 2017), the aforementioned cratons and terrane formed two continental collages (Fig. 12b): (1) São Francisco–Congo–West African–Afif–Abas;

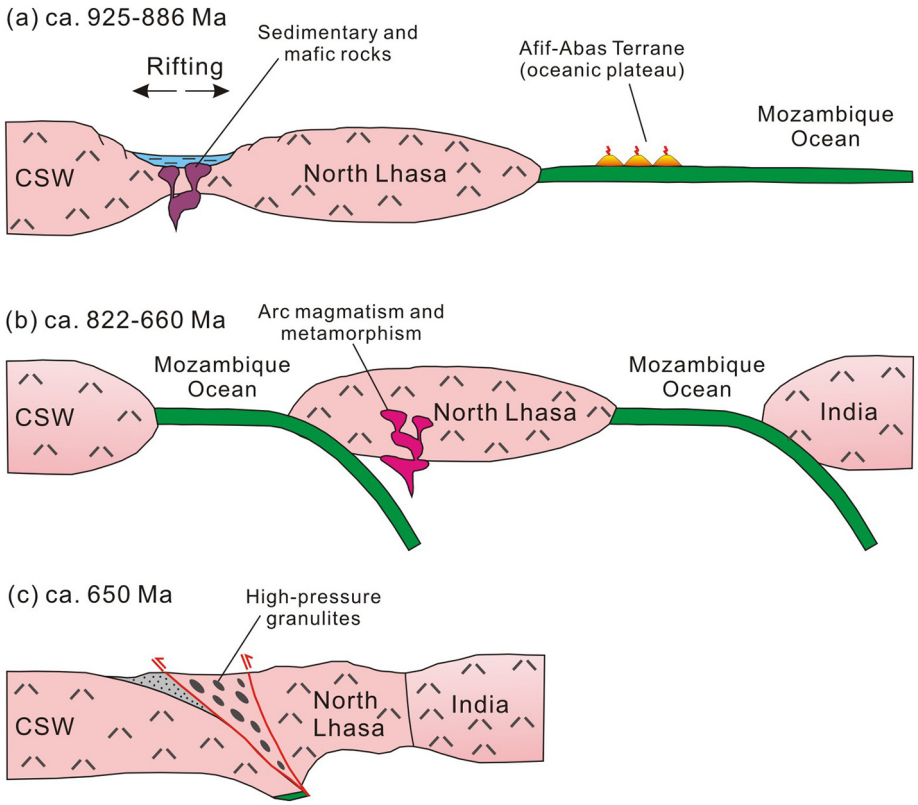

Fig. 13. Schematic tectonic evolution of the North Lhasa Terrane during the Neoproterozoic. See text for explanation. CSW = Congo, São Francisco, and West African cratons.

and (2) Tarim–North China. Detrital zircons with ages of 1200–1000 Ma are rare in the Neoproterozoic sediments of the Tarim–North China continental collage (Fig. 10i and j) and, as such, the North Lhasa Terrane could not have been part of this continental collage.

In summary, we speculate that the North Lhasa Terrane originated from the African side of the northern EAO because of the: (1) distinctive 1200–1000 Ma age population of detrital zircons (Zhu et al., 2011a; this study); (2) middle Neoproterozoic arc-related magmatism and metamorphism (ca. 822–660 Ma; Dong et al., 2011; Zhang et al., 2013; Hu et al., 2018b) and collision-related high-pressure metamorphism (ca. 650 Ma; Zhang et al., 2012); (3) relatively prolonged Ediacaran–early Paleozoic (ca. 568–488 Ma) Andean-type magmatism (Hu et al., 2018a and references therein); and (4) early Neoproterozoic rifting event (ca. 900 Ma; this study) in this terrane. The North Lhasa Terrane may not come from India or Australia, because these two continents do not have Ediacaran Andean-type and early Neoproterozoic rifting-related magmatism and the Australia is characterized by lack of middle Neoproterozoic arc-related magmatism and metamorphism.

5.4.2. Neoproterozoic geodynamic evolution of the North Lhasa Terrane

Here we integrate the Neoproterozoic geological record of the North Lhasa Terrane and the history of rift sedimentation and mafic magmatism documented in this paper, and propose for the first time that a Wilson cycle occurred during ca. 925–650 Ma (Fig. 13). During the early Neoproterozoic (ca. 925–886 Ma), N-MORB-like magmatism (Zhang et al., 2012; Hu et al., 2016; this study) occurred in the North Lhasa Terrane in response to the final stages of a rift (Fig. 13a). Coeval sedimentary rocks in the rift basin incorporated a large amount of ca. 1200–1000 Ma detrital zircons from African cratons. This rift probably finally formed an oceanic basin, as suggested by the ca. 850 Ma MORB-like rocks in the North Lhasa Terrane (Dong et al., 2011). During the middle Neoproterozoic (ca. 822–660 Ma), arc-related basaltic rocks (ca. 822–806 Ma, Hu et al., 2018b; ca. 760 Ma, Hu et al., 2018c; ca. 742 Ma; Zhang et al., 2013) were generated and metamorphism (ca. 680–660 Ma, Dong et al., 2011; ca. 666 Ma, Zhang et al., 2013) occurred in the North Lhasa Terrane, related to subduction of oceanic lithosphere, which marked the suturing of this oceanic basin (Fig. 13b). High-pressure metamorphism at ca. 650 Ma, which is typical of a collision zone, represented the final closure of the oceanic basin (Zhang et al., 2012) (Fig. 13c). Subsequently, the North Lhasa Terrane was influenced by Ediacaran–early Paleozoic (568–488 Ma) Andean-type magmatism along the proto-Tethyan margin of Gondwana (Hu et al., 2018a) (Fig. 11).

Previous studies have indicated that oceanic subduction occurred adjacent to Madagascar (Archibald et al., 2018), Sri Lanka (He et al., 2016), and East Antarctica (Jacobs et al., 2015) at ca. 900 Ma, and so the Mozambique Ocean had already formed by this time. Therefore, the Neoproterozoic oceanic basin probably represented a branch of the Mozambique Ocean, which was adjacent to eastern Africa. Our interpretations are based primarily on the limited data currently available for the Neoproterozoic geology of the North Lhasa Terrane and, as such, further research is required to test our hypothesis.

6. Conclusions

(1) Zircon U—Pb dating of amphibolites and quartzites from the North Lhasa Terrane has revealed that early Neoproterozoic sedimentation and mafic magmatism occurred at ca. 900 Ma. The detrital zircons in the quartzites are characterized by a main age population of 1200–1000 Ma and an absence of 1000–900 Ma ages.

(2) The amphibolites have N-MORB-like compositions and are characterized by high positive zircon $\varepsilon_{Hf}(t)$ (+7.2 to +14.0) and whole-rock $\varepsilon_{Nd}(t)$ (+5.5 to +6.0) values. The amphibolite protoliths were most likely derived from relatively high degrees of partial melting (>20%) of spinel lherzolite with a depleted mantle composition. These basaltic magmas were modified by crustal contamination.

(3) The formation of these quartzites and amphibolites was related to an early Neoproterozoic rift adjacent to the African side of the northern EAO, which was associated with the opening of a branch of the Mozambique Ocean.

Acknowledgments

This study was supported by the Ministry of Science and Technology of China (Grant No. 2016YFC0600304), National Science Foundation of China (Grant No. 41522204, 41502216, 91755103, and 41872240), the Institute of Geology of the Chinese Academy of Geological Sciences (Grant No. J1705 and YYWF201704), and the Chinese Geological Survey Project (Grant No. DD20160123-05 and DD20160345).

Appendix A. Supplementary data

Supplementary data to this article can be found online at https://doi.org/10.1016/j.lithos.2018.09.036.

References

Allègre, C.J., Courtillot, V., Tapponnier, P., Hirn, A., Mattauer, M., Coulon, C., Jaeger, J.J., Achache, J., Scharer, U., Marcoux, J., Burg, J.P., Girardeau, J., Armijo, R., Gariepy, C., Gopel, C., Li, T.D., Xiao, X.C., Chang, C.F., Li, G.Q., Lin, B.Y., Teng, J.W., Wang, N.W., Chen, G.M., Han, T.L., Wang, X.B., Den, W.M., Sheng, H.B., Cao, Y.G., Zhou, J., Qiu, H.R., Bao, P.S., Wang, S.C., Wang, B.X., Zhou, Y.X., Ronghua, X., 1984. Structure and evolution of the Himalaya–Tibet Orogenic Belt. Nature 307, 17–22.

Álvaro, J.J., Pouclet, A., Ezzouhairi, H., Soulaimani, A., Bouougri, E.H., Imaz, A.G., Fekkak, A., 2014. Early Neoproterozoic rift-related magmatism in the Anti-Atlas margin of the West African craton, Morocco. Precambrian Research 255, 433–442.

Archibald, D., Collins, A.S., Foden, J., Payne, J.L., Macey, P., Holden, P., Razakamanana, T., 2018. Stenian-Tonian arc magmatism in west central Madagascar: Genesis of the Dabolava Suite. Journal of the Geological Society 175, 111–129.

Audley-Charles, M.G., 1984. Cold Gondwana, warm Tethys and the Tibetan Lhasa block. Nature 310, 165–166.

Bicca, M.M., Jelinek, A.R., Philipp, R.P., Lana, C.D.C., Alkmim, A.R., 2018. Precambrian-Cambrian provenance of Matinde Formation, Karoo Supergroup, northwestern Mozambique, constrained from detrital zircon U-Pb age and Lu-Hf isotope data. Journal of African Earth Sciences 138, 42–57.

Cawood, P.A., Nemchin, A.A., 2000. Provenance record of a rift basin: U/Pb ages of detrital zircons from the Perth Basin, Western Australia. Sedimentary Geology 134, 209–234.

Cawood, P.A., Hawkesworth, C.J., Dhuime, B., 2012. Detrital zircon record and tectonic setting. Geology 40, 875–878.

Chauvet, F., Lapierre, H., Bosch, D., Guillot, S., Mascle, G., Vannay, J.C., Cotten, J., Brunet, P., Keller, F., 2008. Geochemistry of the Panjal Traps basalts (NW Himalaya): records of the Pangea Permian break-up. Bulletin de la Société Géologique de France 179 (4), 383–395.

Chen, S.Y., Yang, J.S., Li, Y., Xu, X.Z., 2009. Ultramafic Blocks in Sumdo Region, Lhasa Block, Eastern Tibet Plateau: an Ophiolite Unit. Journal of Earth Science 20, 332–347.

Chen, S.S., Shi, R.D., Fan, W.M., Gong, X.H., Wu, K., 2017. Early Permian mafic dikes in the Nagqu area, central Tibet, China, associated with embryonic oceanic crust of the Meso-Tethys Ocean. J. Geophys. Res. 122, 4172–4190.

Clark, D.J., Hensen, B.J., Kinny, P.D., 2000. Geochronological constraints for a two-stage history of the Albany-Fraser orogen, Western Australia. Precambrian Research 102, 155–183.

Correa-Gomes, L.C., Oliveira, E.P., 2000. Radiating 1.0 Ga mafic dyke swarms of eastern Brazil and western Africa: evidence of post-assembly extension in the Rodinia supercontinent? Gondwana Research 3, 325–332.

Collins, A.S., Fitzsimons, I.C.W., Hulscher, B., Razakamanana, T., 2003. Structure of the eastern margin of the East African Orogen in Central Madagascar. Precambrian Research 123, 111–133.

Corfu, F., Hanchar, J.M., Hoskin, P.W.O., Kinny, P., 2003. Atlas of zircon textures. Reviews in Mineralogy and Geochemistry 53, 469–500.

Dilek, Y., Furnes, H., 2011. Ophiolite genesis and global tectonics: geochemical and tectonic fingerprinting of ancient oceanic lithosphere. GSA Bulletin 123, 387–411.

Doebrich, J.L., Al-Jehani, A.M., Siddiqui, A.A., Hayes, T.S., Wooden, J.L., Johnson, P.R., 2007. Geology and metallogeny of the Ar Rayn terrane, eastern Arabian shield: Evolution of a Neoproterozoic continental-margin arc during assembly of Gondwana within the East African orogen. Precambrian Research 158, 17–50.

Dong, X., Zhang, Z.M., Santosh, M., Wang, W., Yu, F., Liu, F., 2011. Late Neoproterozoic thermal events in the northern Lhasa terrane, South Tibet: zircon chronology and tectonic implications. Journal of Geodynamics 52, 389–405.

Dong, X.P., Hu, J.M., Li, Z.H., Zhao, Y., Gong, W.B., Yang, Y., 2017. Provenance of Ediacaran (Sinian) sediments in the Helanshan area, North China Craton: Constraints from U–Pb geochronology and Hf isotopes of detrital zircons. Precambrian Research 298, 490–511.

D'Orazio, M., Agostini, S., Innocenti, F., Haller, M.J., Manetti, P., Mazzarini, F., 2001. Slab window-related magmatism from southernmost South America: the late Miocene mafic volcanics from the Estancia Glencross area (~52°S, Argentina–Chile). Lithos 57, 67–89.

Evans, D., Trindade, R., Catelani, E., D'Agrella-Filho, M.S., Heaman, L.M., Oliveira, E.P., Söderlund, U., Ernst, R.E., Smirnov, A.V., Salminen, J.M., 2015. Return to Rodinia? Moderate to High Paleolatitude of the Sao Francisco/Congo Craton at 920 Ma. In: Li, Z.-X., Evans, D.A.D., Murphy, J.B. (Eds.), Supercontinent Cycles through Earth History. vol. 424. Geological Society of London, London. https://doi.org/10.1144/SP424.1 Special Publication.

Fitton, J.G., 2007. The OIB paradox. In: Foulger, G.R., Jurdy, D.M. (Eds.), Plates, Plumes, and Planetary Processes. vol. 430. Geol. Soc. Am. Spec. Papl., pp. 387–412.

Franssen, L., André, L., 1988. The Zadinian group (late Proterozoic, Zaire) and its bearing on the origin of the West-Congo orogenic belt. Precambrian Research 38, 215–234.

Fritz, H., Abdelsalam, M., Ali, K.A., Bingen, B., Collins, A.S., Fowler, A.R., Ghebreab, W., Hauzenberger, C.A., Johnson, P.R., Kusky, T.M., Macey, P., Muhongo, S., Stern, R.J., Viola, G., 2013. Orogen styles in the East African Orogen: a review of the Neoproterozoic to Cambrian tectonic evolution. Journal of African Earth Sciences 86, 65–106.

Gehrels, G., Kapp, P., Decelles, P., Pullen, A., Blakey, R., Weislogel, A., Ding, L., Guynn, J., Martin, A., McQuarrie, N., Yin, A., 2011. Detrital zircon geochronology of pre-Tertiary strata in the Tibetan-Himalayan orogen. Tectonics 30, TC5016. https://doi.org/10.1029/2011TC002868.

Govindaraju, K., 1994. 1994 compilation of working values and sample description for 383 geostandards. Geostandards Newsletter 18, 1–158.

He, X.F., Santosh, M., Tsunogae, T., Sanjeewa, P.K.M., Dharmapriya, P.L., 2016. Neoproterozoic arc accretion along the 'eastern suture' in Sri Lanka during Gondwana assembly. Precambrian Research 279, 57–80.

Hoskin, P.W.O., Schaltegger, U., 2003. The composition of zircon and igneous and metamorphic petrogenesis. In: Manchar, J.M., Hoskin, P.W.O. (Eds.), Zircon: Reviews of Mineralogy and Geochemistry. Vol. 53, pp. 27–62.

Hu, P.Y., Zhai, Q.G., Tang, Y., Wang, J., Wang, H.T., 2016. Early Neoproterozoic meta-gabbro (~925 Ma) from the Lhasa terrane, Tibetan Plateau and its geological significance. Chinese Science Bulletin 61, 2176–2186 (in Chinese with English abstract).

Hu, P.Y., Zhai, Q.G., Wang, J., Tang, Y., Wang, H.T., Hou, K.J., 2018a. Ediacaran magmatism in the North Lhasa terrane, Tibet and its tectonic implications. Precambrian Research 307, 137–154.

Hu, P.Y., Zhai, Q.G., Wang, J., Tang, Y., Wang, H.T., Hou, K.J., 2018b. Precambrian origin of the North Lhasa terrane, Tibetan Plateau: Constraint from early Cryogenian back-arc magmatism. Precambrian Research 313, 51–67.

Hu, P.Y., Zhai, Q.G., Wang, J., Tang, Y., Wang, H.T., Zhu, Z.C., Wu, H., 2018c. Middle Neoproterozoic (ca. 760 Ma) arc and back-arc system in the North Lhasa terrane, Tibet, inferred from coeval N-MORB- and arc-type gabbros. Precambrian Research 316, 275–290.

Iizuka, T., Campbell, I.H., Allen, C.M., Gill, J.B., Maruyama, S., Makoka, F., 2013. Evolution of the African continental crust as recorded by U–Pb, Lu–Hf and O isotopes in detrital zircons from modern rivers. Geochimica et Cosmochimica Acta 107, 96–120.

Jackson, S.E., Pearson, N.J., Griffin, W.L., Belousova, E.A., 2004. The application of laser ablation-inductively coupled plasma-mass spectrometry to in situ U-Pb zircon geochronology. Chemical Geology 211, 47–69.

Jacobs, J., Elburg, M., Läufer, A., Kleinhanns, I.C., Henjes-Kunst, F., Estrada, S., Ruppel, A.S., Damaske, D., Montero, P., Bea, F., 2015. Two distinct late Mesoproterozoic/early Neoproterozoic basement provinces in central/eastern Dronning Maud Land, East Antarctica: the missing link, 15–21° E. Precambrian Res. 265, 249–272.

Kalsbeek, F., Frei, D., Affaton, P., 2008. Constraints on provenance, stratigraphic correlation and structural context of the Volta basin, Ghana, from detrital zircon geochronology: an Amazonian connection? Sedimentary Geology 212, 86–95.

Li, X.H., Li, Z.X., Sinclair, J.A., Li, W.X., Garter, G., 2006. Revisiting the "Yanbian Terrane": implications for Neoproterozoic tectonic evolution of the western Yangtze Block, South China. Precambrian Research 151, 14–30.

Lundmark, A.M., Andresen, A., Hassan, M.A., Augland, L.E., Baghdady, G.Y., 2012. Repeated magmatic pulses in the East African Orogen of Central Eastern Desert, Egypt: an old idea supported by new evidence. Gondwana Research 22, 227–237.

McKenzie, N.R., Hughes, N.C., Myrow, P.M., Xiao, S.H., Sharma, M., 2011. Correlation of Precambrian–Cambrian sedimentary successions across northern India and the utility of isotopic signatures of Himalayan lithotectonic zones. Earth and Planetary Science Letters 312, 471–483.

Meert, J., 2003. A synopsis of events related to the assembly of eastern Gondwana. Tectonophysics 362, 1–40.

Merdith, A.S., Collins, A.S., Williams, S.E., Pisarevsky, S., Foden, J.D., Archibald, D.B., Blades, M.L., Alessio, B.L., Armistead, S., Plavsa, D., Clark, C., Müller, R.D., 2017. A full-plate global reconstruction of the Neoproterozoic. Gondwana Research 50, 84–134.

Miyashiro, A., 1974. Volcanic rock series in island arc and active continental margins. American Journal of Science 274, 321–355.

Mole, D.R., Barnes, S.J., Taylor, R.J.M., Kinny, P.D., Fritz, H., 2018. A relic of the Mozambique Ocean in south-east Tanzania. Precambrian Research 305, 386–426.

Pang, C.J., Wang, X.C., Xu, B., Zhao, J.X., Feng, Y.X., Wang, Y.Y., Luo, Z.W., Liao, W., 2016. Late Carboniferous N-MORB-type basalts in Central Inner Mongolia, China: Products of hydrous melting in an intraplate setting? Lithos 261, 55–71.

Peng, P., Bleeker, W., Ernst, R.E., Söderlund, U., McNicoll, V., 2011a. U–Pb baddeleyite ages, distribution and geochemistry of 925 Ma mafic dykes and 900 Ma sills in the North China craton: evidence for a Neoproterozoic mantle plume. Lithos 127, 210–221.

Peng, P., Zhai, M., Li, Q., Wu, F., Hou, Q., Li, Z., Li, T., Zhang, Y., 2011b. Neoproterozoic (900 Ma) Sariwon sills in North Korea: geochronology, geochemistry and implications for the evolution of the south-eastern margin of the North China craton. Gondwana Research 20, 243–254.

Plavsa, D., Collins, A.S., Payne, J.L., Foden, J.D., Clark, C., Santosh, M., 2014. Detrital zircons in basement metasedimentary protoliths unveil the origins of southern India. GSA Bulletin 126, 791–811.
Rudnick, R.L., Fountain, D.M., 1995. Nature and composition of the continental crust: a lower crustal perspective. Reviews of Geophysics 33, 267–309.
Stein, M., 2003. Tracing the plume material in the Arabian-Nubian Shield. Precambrian Research 123, 223–234.
Sun, S.S., McDonough, W.F., 1989. Chemical and isotopic systematics of oceanic basalts: implications for mantle composition and processes. Geol. Soc. Lond. Special Publ. 42, 313–345.
Tack, L., Wingate, M.T.D., Liégeois, J.-P., Fernandez-Alonso, M., 2001. Early Neoproterozoic magmatism (1000–910 Ma) of the Zadinian and Mayumbian groups (Bas-Congo): onset of Rodinia rifting at the western edge of the Congo craton. Precambrian Research 110, 277–306.
Wang, Y.M., Gao, Y.S., Han, H.M., Wang, X.H., 2003. Practical Handbook of Reference Materials for Geoanalysis. Geological Publishing House (in Chinese).
Wang, C.S., Zhao, X.X., Liu, Z.F., Lippert, P.C., Graham, S.A., Coe, R.S., Yi, H.S., Zhu, L.D., Liu, C., Li, Y.L., 2008. Constraints on the early uplift history of the Tibetan Plateau. Proceedings of the National Academy of Sciences of the United States of America 105, pp. 4987–4992.
Wang, C., Zhang, J.H., Li, M., Li, R.S., Peng, Y., 2015. Generation of ca. 900–870 Ma bimodal rifting volcanism along the southwestern margin of the Tarim Craton and its implications for the Tarim–North China connection in the early Neoproterozoic. Journal of Asian Earth Sciences 113, 610–625.
Wang, W., Pandit, M.K., Zhao, J.H., Chen, W.T., Zheng, J.P., 2018. Slab break-off triggered lithosphere–asthenosphere interaction at a convergent margin: the Neoproterozoic bimodal magmatism in NW India. Lithos 296 (299), 281–296.
Weyer, S., Münker, C., Mezger, K., 2003. Nb/Ta, Zr/Hf and REE in the depleted mantle: Implications for the differentiation history of the crust–mantle system. Earth and Planetary Science Letters 205 (3), 309–324.
Winchester, J.A., Floyd, P.A., 1977. Geochemical discrimination of different magma series and their differentiation products using immobile elements. Chemical Geology 20, 325–343.
Woodhead, J.D., Hergt, J.M., 2005. A preliminary appraisal of seven natural zircon reference materials for in situ Hf isotope determination. Geostandards and Geoanalytical Research 29, 183–195.
Wu, C., Zuza, A.V., Yin, A., Liu, C.F., Reith, R.C., Zhang, J.Y., Liu, W.C., Zhou, Z.G., 2017. Geochronology and geochemistry of Neoproterozoic granitoids in the central Qilian Shan of northern Tibet: Reconstructing the amalgamation processes and tectonic history of Asia. Lithosphere 9, 609–636.
Wu, F.Y., Yang, Y.H., Xie, L.W., Yang, J.H., Ping, C., 2006. Hf isotopic compositions of the standard zircons and baddeleyites used in U-Pb geochronology. Chemical Geology 234, 105–126.
Xu, M.J., Li, C., Zhang, X.Z., Wu, Y.W., 2014. Nature and evolution of the Neo-Tethys in Central Tibet: synthesis of ophiolitic petrology, geochemistry, and geochronology. International Geology Review 56, 1072–1096.
Yang, J.S., Xu, Z.Q., Li, Z.L., Xua, X.Z., Li, T.F., Ren, Y.F., Li, H.Q., Chen, S.Y., Robinson, P.T., 2009. Discovery of an eclogite belt in the Lhasa block, Tibet: a new border for Paleo-Tethys? Journal of Asian Earth Sciences 34, 76–89.
Yin, A., Harrison, T.M., 2000. Geologic evolution of the Himalayan–Tibetan orogen. Annual Review of Earth and Planetary Sciences 28, 211–280.
Zhai, Q.G., Jahn, B.M., Wang, J., Su, L., Mo, X.X., Wang, K.L., Tang, S.H., Lee, H.Y., 2013. The Carboniferous ophiolite in the middle of the Qiangtang terrane, Northern Tibet: SHRIMP U-Pb dating, geochemical and Sr–Nd–Hf isotopic characteristics. Lithos 168–169 (1–2), 173–189.
Zhang, Z.M., Dong, X., Liu, F., Lin, Y., Yan, R., He, Z., Santosh, M., 2012. The making of Gondwana: discovery of 650 Ma HP granulites from the North Lhasa, Tibet. Precambrian Res. 212 (213), 107–116.
Zhang, X.Z., Dong, Y.S., Li, C., Xie, C.M., Yang, H.T., Wang, M., 2013. Delineation of Middle Neoproterozoic ophiolite mélange in the northern Lhasa terrane, South Tibet and its significance. Acta Petrologica Sinica 29, 698–722 (in Chinese with English abstract).
Zhang, C.L., Ye, X.T., Zou, H.B., Chen, X.Y., 2016. Neoproterozoic sedimentary basin evolution in southwestern Tarim, NW China: New evidence from field observations, detrital zircon U–Pb ages and Hf isotope compositions. Precambrian Research 280, 31–45.
Zhu, D.C., Mo, X.X., Zhao, Z.D., Niu, Y.L., Wang, L.Q., Chu, Q.H., Pan, G.T., Xu, J.F., Zhou, C.Y., 2010. Presence of Permian extension- and arc-type magmatism in southern Tibet: paleogeographic implications. GSA Bulletin 122 (7–8), 979–993.
Zhu, D.C., Zhao, Z.D., Niu, Y., Dilek, Y., Mo, X.X., 2011a. Lhasa terrane in southern Tibet came from Australia. Geology 39, 727–730.
Zhu, D.C., Zhao, Z.D., Niu, Y.L., Mo, X.X., Chung, S.L., Hou, Z.Q., Wang, L.Q., Wu, F.Y., 2011b. The Lhasa Terrane: record of a microcontinent and its histories of drift and growth. Earth and Planetary Science Letters 301, 241–255.
Zhu, D.C., Zhao, Z.D., Niu, Y., Dilek, Y., Hou, Z.Q., Mo, X.X., 2013. The origin and preCenozoic evolution of the Tibetan Plateau. Gondwana Research 23, 1429–1454.